

Pt/CeO₂-ZrO₂-La₂O₃柴油车尾气氧化催化剂活性及抗硫性能

钟富兰, 钟喻娇, 肖益鸿, 蔡国辉, 郑 勇, 魏可镁*

福州大学化肥催化剂国家工程研究中心, 福建福州 350002

摘要: 采用两种方法制备了三种Pt/CeO₂-ZrO₂-La₂O₃柴油车尾气氧化催化剂, 并用X射线衍射、N₂物理吸附、程序升温还原、程序升温脱附、X射线荧光光谱和红外光谱等方法对其进行了表征。结果发现, 制备方法对催化剂的结构、织构、抗硫性能及催化性能的影响非常大。对其进行硫中毒, 导致起燃温度明显升高。将ZrO₂和La₂O₃沉积在CeO₂表面所制得的Pt/CeO₂-ZrO₂-La₂O₃催化剂表现出更高的抗硫及催化氧化性能, 这主要归功于Pt在富Zr载体表面具有更高的分散性。

关键词: 氧化铈; 氧化锆; 氧化镧; 铂; 沉积沉淀; 硫中毒; 柴油车尾气净化

中图分类号: O643 文献标识码: A

收稿日期: 2011-04-18. 接受日期: 2011-06-03.

*通讯联系人. 电话/传真: (0591)83770818; 电子信箱: wei-kemei@163.com

基金来源: 国家科技支撑计划(2007BAE08B01)。

本文的英文电子版(国际版)由Elsevier出版社在ScienceDirect上出版(<http://www.sciencedirect.com/science/journal/18722067>)。

Sulfur Resistance and Activity of Pt/CeO₂-ZrO₂-La₂O₃ Diesel Oxidation Catalysts

ZHONG Fulan, ZHONG Yujiao, XIAO Yihong, CAI Guohui, ZHENG Yong, WEI Kemei*

National Engineering Research Center of Chemical Fertilizer Catalyst, Fuzhou University, Fuzhou 350002, Fujian, China

Abstract: Three Pt/CeO₂-ZrO₂-La₂O₃ diesel oxidation catalysts were prepared by two different routes and characterized by X-ray diffraction, N₂ adsorption, temperature-programmed reduction, temperature-programmed desorption, X-ray photoelectron spectroscopy, and infrared spectroscopy. The synthesis procedure affected the structure, texture, sulfur resistance, and catalytic activity of the catalysts. Sulfur poisoning increased the light-off temperature of all the catalysts, but the Pt/CeO₂-ZrO₂-La₂O₃ catalyst prepared by depositing ZrO₂ and La₂O₃ on the surface of CeO₂ nanoparticles exhibited better sulfur tolerance and catalytic activity with simulated diesel emission due to the high dispersion of Pt on CeO₂-ZrO₂-La₂O₃ oxide with a Zr-rich surface.

Key words: ceria; zirconia; lanthana; platinum; deposition-precipitation; sulfur-poisoning; diesel exhaust purification

Received 18 April 2011. Accepted 3 June 2011.

*Corresponding author. Tel/Fax: +86-591-83770818; E-mail: wei-kemei@163.com

This work was supported by the National Key Technology R&D Program (2007BAE08B01).

English edition available online at Elsevier ScienceDirect (<http://www.sciencedirect.com/science/journal/18722067>).

Diesel engines are widely used in automotive vehicles because of their high fuel efficiency and low NO_x production as compared to gasoline engines [1]. The lean combustion of diesel engine contributes to good fuel economy, but it also results in a low emission temperature. This is bad for the elimination of diesel pollutant gases, which are mainly carbon monoxide, hydrocarbons, and particulate matter (PM) that contains elemental carbon (ca. 31%), sulphates and moisture (ca. 14%), unburnt fuel (ca. 7%), lubricant oil

(ca. 40%), and metals [2]. Among several post-treatment technologies used for diesel exhaust gases, catalytic oxidation by diesel oxidation catalysts (DOCs) working in excess oxygen is a promising solution [3–6]. However, many studies [7–9] have shown that although both Pd and Pt-based DOCs exhibit high initial activity, they are easily deactivated. Sulfur or impurity poisoning of the catalysts has been proposed in previous studies [10–13]. Therefore, improving the sulfur tolerance of DOCs is of great concern.

The choice of the support is important for preparing highly efficient and sulfur-tolerant DOCs. Compared to inert catalyst supports such as Al_2O_3 and SiO_2 , ceria-based materials can create “active oxygen” [14], and thus reduce the light-off temperature of contaminant oxidation over DOCs. A large number of studies have shown that the use of CeO_2 -based materials as the support for Pt-based DOCs accelerated the oxidation rate of diesel soot due to the high availability of surface oxygen and high surface reducibility [10,15,16], but these catalysts were easily sulfated during the removal of the pollutants in diesel exhaust gas since SO_2 was present and blocked active sites. Bazin et al. [17] reported that the addition of zirconia to ceria limited sulfiding in the bulk of the oxide, and thereby reduced the total sulfur uptake. Rohart et al. [18] also reported that the quantity of sulfate adsorption on ceria-rich oxide was more than on zirconia-rich oxides as a result of strong surface basicity. This suggested that the sulfur resistance of $\text{CeO}_2\text{-ZrO}_2$ materials can be tuned by modifying the surface composition.

It is well-known that the preparation method and the CeO_2 component of $\text{CeO}_2\text{-ZrO}_2$ materials can give different crystalline phases including three stable phases (monoclinic (*m*), tetragonal (*t*), cubic (*c*)), and two metastable phases (*t'*, *t''*) [10,19], and also give significant differences in thermal, chemical, and redox properties. Our previous study [20] showed that the incorporation of La_2O_3 into $\text{CeO}_2\text{-ZrO}_2$ oxide can effectively improve its thermal and chemical properties, which are key parameters that determine the potential application of $\text{CeO}_2\text{-ZrO}_2$ materials in the removal of pollutants in exhaust gases from vehicles. In the present work, thermally stable $\text{CeO}_2\text{-ZrO}_2\text{-La}_2\text{O}_3$ ternary oxides were first prepared using two frequently used synthesis routes for fabricating heterogeneous catalysts, that is, deposition-precipitation and co-precipitation methods. These were used as the support of Pt-based DOCs for the simultaneous oxidation of CO and C_3H_6 . The structure, texture, and surface properties of the catalysts were characterized in detail by X-ray diffraction (XRD), N_2 adsorption, temperature-programmed reduction (TPR), temperature-programmed desorption (TPD), X-ray photoelectron spectroscopy (XPS), and infrared (IR) spectroscopy. The emphasis was on the comparison of the sulfur resistance of the catalysts prepared by the two methods in order to develop practical $\text{CeO}_2\text{-ZrO}_2$ -based DOCs with a low light-off temperature.

1 Experimental

1.1 Catalyst preparation

The $\text{CeO}_2\text{-ZrO}_2\text{-La}_2\text{O}_3$ materials were prepared by two methods: deposition-precipitation and co-precipitation. For

deposition-precipitation method, the required amount of $\text{Ce}(\text{NO}_3)_3\cdot 6\text{H}_2\text{O}$ was first calcined at 573 K for 4 h to obtain CeO_2 particles with a high surface area. A slurry was obtained by ball-milling the CeO_2 with some deionized water for several hours. The required amount of ammonia solution was added into the slurry. A stoichiometric mixture of $\text{ZrOCl}_2\cdot 8\text{H}_2\text{O}$ and $\text{La}(\text{NO}_3)_3\cdot 6\text{H}_2\text{O}$ solutions ($\text{Ce}:\text{Zr}:\text{La} = 5:4:1$, molar ratio) was used to deposit the CeO_2 particles. The pH of solution was controlled at 9.0. The resulting precipitates were filtered, washed with distilled water, dried, and calcined at 873 K for 4 h in air. The resulting $\text{CeO}_2\text{-ZrO}_2\text{-La}_2\text{O}_3$ was denoted as A.

After ball-milling the ZrO_2 particles with an amount of deionized water for several hours, the required amount of ammonia solution was added into the slurry. A stoichiometric mixture of $\text{Ce}(\text{NO}_3)_3\cdot 6\text{H}_2\text{O}$ and $\text{La}(\text{NO}_3)_3\cdot 6\text{H}_2\text{O}$ solutions was used to deposit the milled ZrO_2 particles. The pH of solution was controlled at 9.0. The resulting precipitates were filtered, washed with distilled water, dried, and calcined at 873 K for 4 h in air. The $\text{CeO}_2\text{-ZrO}_2\text{-La}_2\text{O}_3$ oxide obtained with the same composition as A was denoted as B. The ZrO_2 particles were prepared by precipitation with ammonia from a solution of $\text{ZrOCl}_2\cdot 8\text{H}_2\text{O}$, which was followed by washing, drying at 383 K for 15 h, and calcination at 823 K for 4 h.

For co-precipitation method, the mixed aqueous solution of $\text{Ce}(\text{NO}_3)_3\cdot 6\text{H}_2\text{O}$, $\text{ZrOCl}_2\cdot 8\text{H}_2\text{O}$, and $\text{La}(\text{NO}_3)_3\cdot 6\text{H}_2\text{O}$ was quickly dropped into ammonia solution and the pH of solution was controlled at 9.0. The precipitate obtained was filtered, washed with distilled water, dried, and calcined at 873 K in air. The resulting $\text{CeO}_2\text{-ZrO}_2\text{-La}_2\text{O}_3$ oxide was denoted as C (with the same molar composition as A and B).

The loading of platinum on the $\text{CeO}_2\text{-ZrO}_2\text{-La}_2\text{O}_3$ oxides was carried out by impregnation using a solution of $\text{H}_2\text{PtCl}_6\cdot 6\text{H}_2\text{O}$. The resultant solids were calcined at 873 K for 4 h in air. The catalysts obtained were marked as Pt/A, Pt/B, and Pt/C. The Pt/A-S, Pt/B-S, and Pt/C-S denoted the sulfated catalysts. The Pt/A-R, Pt/B-R, and Pt/C-R denoted the regenerated catalysts. The loading of platinum was determined by a Axios Petro X-Ray fluorescence (XRF) spectrometer.

For comparison, the $\text{Pt}/\text{Al}_2\text{O}_3$ catalyst was also prepared. Al_2O_3 was obtained by precipitation with the required amount of ammonia and NH_4HCO_3 from a solution of $\text{Al}(\text{NO}_3)_3\cdot 9\text{H}_2\text{O}$, followed by washing, drying for 15 h at 383 K, and calcination at 873 K for 4 h.

1.2 Catalyst characterization

XRD data were recorded on a Panalytical X’Pert Pro diffractometer at 40 kV and 40 mA with a step of 0.0167° at a

scanning rate of 10°/min using Co K_α radiation, which was then revised to Cu K_α. The specific surface areas and pore size distribution of the samples were determined on a TriStar 3000 apparatus by N₂ adsorption at 77 K. The samples were outgassed in vacuum at 300 °C for more than 3 h until the residual pressure was less than 1333 Pa before the adsorption. XPS spectra were collected on a VG ESCALAB 250 XPS system with a monochromatized Al K_α X-ray source (15 kV, 200 W, 500 μm, pass energy = 20 eV). All binding energies were calibrated using the C 1s peak at 284.6 eV.

The CO-TPD experiments were performed on an AutoChem 2920 instrument by the pulse technique. About 100 mg of samples were placed in a quartz tube and pretreated at 773 K in flowing H₂ for 30 min, then in flowing He for 20 min, and subsequently cooled to room temperature in He. The reduced samples were pulsed with CO at an interval of 3 min until the intensity of the peak was constant. The temperature of the sample was then raised from room temperature to 1123 K at a rate of 10 K/min. The metal dispersion was determined by the amount of CO consumed during the pulse.

The desulfiding characteristics were analyzed with a quadrupole mass spectrometer (Ametek Process Instruments, Model Dycor DM100M). The powder samples were sulfated by exposure to a feed containing 0.04% SO₂, 13% O₂, and balance He (feed rate of 200 ml/min) for 30 min at 623 K. The catalysts were then subjected to desulfiding under 10% H₂-90% He by raising the temperature from 563 to 873 K at a rate of 3 K/min.

1.3 Activity test

Catalytic activity tests for the oxidation of CO and C₃H₆ were carried out on a fixed-bed continuous flow reactor. The catalyst (0.1 g) was held in a quartz glass tube reactor (i.d. 10.5 mm) equipped with a temperature-programmed controller. Prior to measurement, the catalyst was pretreated in 1% CO-99% He at 673 K for 0.5 h. For the sulfated sample, the powder samples were sulfated by exposure to a feed containing 0.04% SO₂, 13% O₂, and balance He (feed rate of 200 ml/min) for 30 min at 623 K. The amount of SO₂ adsorbed was determined by XRF. The sulfated samples were regenerated in situ in a H₂ atmosphere at 823 K for 1 h. The reaction gas was a mixture of 0.1% CO, 0.01% C₃H₆, 13.5% O₂, and balance He. The total flow rate of the reaction gas was 200 ml/min (GHSV = 170000 h⁻¹). The catalytic activity was measured while the temperature was raised from 343 to 513 K at a rate of 10 K/min. CO and C₃H₆ compositions in the gas were monitored by two gas chromatographs, GC-14C and 9750, equipped with a thermal conduction detector (TCD) and flame ionization detector (FID), respectively.

$$\text{CO conversion} = (C_{\text{CO, inlet}} - C_{\text{CO, outlet}})/C_{\text{CO, inlet}}$$

$$\text{C}_3\text{H}_6 \text{ conversion} = (C_{\text{C}_3\text{H}_6, \text{ inlet}} - C_{\text{C}_3\text{H}_6, \text{ outlet}})/C_{\text{C}_3\text{H}_6, \text{ inlet}}$$

where $C_{i, \text{inlet}}$ is the concentration of compound i at the reactor inlet and $C_{i, \text{outlet}}$ is that at the reactor outlet.

2 Results and discussion

2.1 Structure and texture of Pt/CeO₂-ZrO₂-La₂O₃ samples before and after sulfur treatment

Figure 1 displays the XRD patterns of the Pt/A, Pt/B, Pt/C, Pt/A-S, Pt/B-S, and Pt/C-S samples. All samples did not show any Bragg diffractive peak of metal Pt or Pt oxide. This was because the loading of Pt (0.5 wt% in Table 1) was too low. For the Pt/A sample prepared by the deposition of ZrO₂ and La₂O₃ on CeO₂ nanoparticles, all the Bragg diffractive peaks were indexed to a mixed tetragonal (JCPDS 38-1436) and cubic (JCPDS 38-1439) phase. Peaks of lanthana and zirconia oxides were not seen, suggesting that La and Zr cations were either incorporated into the ceria lattice or were well dispersed on the ceria surface in the form of amorphous lanthana and zirconia oxides. For the Pt/B sample prepared by the deposition of CeO₂ and La₂O₃ on ZrO₂ nanoparticles, the main diffraction peaks were indexed as the cubic phase. Some weak impurity peaks indexed as the monoclinic phase of ZrO₂ was detected, indicating that ZrO₂ was not fully incorporated into the CeO₂ lattice after calcination at 873 K. A fraction of the ZrO₂ existed as a separated monoclinic phase. These results suggested that the CeO₂-ZrO₂-La₂O₃ supports prepared by the deposition-precipitation method were composed of mixed phases, which depended on the deposition procedure. However, the Pt/C sample prepared by co-precipitation had a single cubic fluorite structure, as indicated by the XRD pattern that was very close to that of CeO₂. Moreover, the lattice parameter

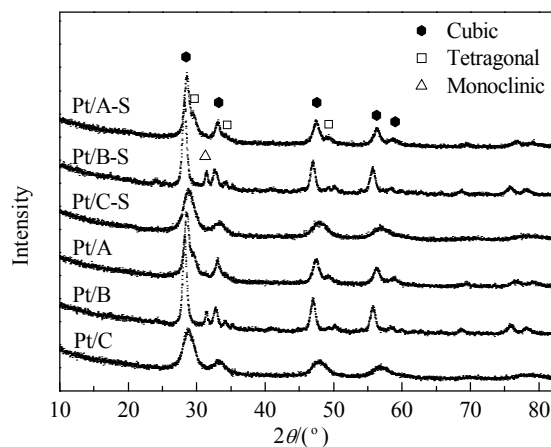


Fig. 1. XRD patterns of the non-sulfated and sulfated Pt/CeO₂-ZrO₂-La₂O₃ catalysts.

Table 1 Physicochemical properties of the Pt/CeO₂-ZrO₂-La₂O₃ and Pt/Al₂O₃ catalysts before and after sulfiding

Sample	$A_{\text{BET}}/(\text{m}^2/\text{g})$	Pore Size (nm)	Pore Volume (cm ³ /g)	Pt content ^a (wt%)	SO ₂ content ^a (wt%)	Metal dispersion (%)	a^{b}/nm
Pt/A	45.4	5.32	0.139	0.56	—	96.45	0.542
Pt/B	49.6	6.46	0.191	0.53	—	82.51	0.546
Pt/C	67.8	1.85	0.077	0.52	—	78.97	0.535
Pt/A-S	20.9	6.26	0.099	0.51	0.95	6.97	0.541
Pt/B-S	26.3	6.81	0.145	0.53	1.48	4.20	0.547
Pt/C-S	34.1	1.71	0.042	0.48	1.10	4.08	0.529
Pt/Al ₂ O ₃	198.4	4.22	0.563	0.50	—	65.89	—
Pt/Al ₂ O ₃ -S	194.2	4.19	0.530	0.49	0.94	35.67	—
Pt/A-R	—	—	—	—	—	7.92	—
Pt/B-R	—	—	—	—	—	5.02	—
Pt/C-R	—	—	—	—	—	4.97	—
Pt/Al ₂ O ₃ -R	—	—	—	—	—	34.30	—

^aDetermined by XRF.^bCalculated according to the (111) facets of the cubic phase.

(a) value for the Pt/B sample was significantly increased by the doping of La³⁺ (ionic radius of La³⁺ = 0.116 nm) [21], while the lattice parameter (a) value of the Pt/A sample was comparable with that of CeO₂ (ca. 0.540 nm), suggesting that considerable amounts of Zr⁴⁺ (ionic radius of Zr⁴⁺ = 0.084 nm) [19] were doped into the CeO₂ fluorite lattice in the case of the Pt/A sample. This caused a drastic difference in the surface atomic composition, which was confirmed by XPS results discussed below.

After sulfur treatment, we did not observe any modifications of the XRD patterns for the Pt/A-S, Pt/B-S, and Pt/C-S samples. This indicated that the sulfiding did not alter their crystalline structure. This was possibly because the pre-treatment time was relatively short, such that the sulfate accumulated was below the detection limit, or the sulfate formed was well dispersed on the catalyst surface. However, the sulfiding significantly changed the texture of the samples, as shown by N₂ adsorption-desorption measurements (Table 1). The BET surface area and pore volume of the sulfated samples decreased by 50% and 30%, respectively, implying the bonding of SO₂ on the surface of the CeO₂-ZrO₂-La₂O₃ support. It is interesting to note that the texture of the reference catalyst (Pt/Al₂O₃) was not altered by sulfur poisoning due to the high SO₂ adsorption capacity [22]. In addition, the physicochemical properties of Al₂O₃ were also completely different from those of the CeO₂-based oxide. The CeO₂-based oxide was alkaline and exhibited the unique feature of the storage and release of oxygen, which helped the adsorption and oxidation of SO₂, thus changing the structure. The XRF results showed that the amount of sulfur adsorbed on the Pt/A-S sample was comparable to that on Pt/Al₂O₃-S, and lower than those of the Pt/B-S and Pt/C-S samples. This indicated that the Pt/A sample had better sulfur resistance.

2.2 Catalytic activity of the Pt/CeO₂-ZrO₂-La₂O₃ samples

Figure 2 shows the conversion curves of CO and C₃H₆ over the Pt/A, Pt/B, Pt/C, and Pt/Al₂O₃ before and after sulfur treatment. The Pt/A catalyst exhibited the best activities for both CO and C₃H₆ oxidation among the catalysts investigated. It gave values of T_{50} (384 K for CO conversion and 403 K for C₃H₆ oxidation), which were lower than those from the Pt/B (407 K for CO conversion and 416 K for C₃H₆ oxidation) and the Pt/C (398 K for CO conversion and 417 K for C₃H₆ oxidation) catalysts. Overall, the non-sulfated Pt/A was better in oxidation catalytic activity as compared with the commercial Pt/Al₂O₃ sample (394 K for CO conversion and 403 K for C₃H₆ oxidation). After sulfur treatment, the light-off temperatures of CO and C₃H₆ oxidation over all the Pt/CeO₂-ZrO₂-La₂O₃ catalysts were increased significantly, while the Pt/A-S catalyst still exhibited a low light-off temperature (423 K for CO conversion and 433 K for C₃H₆ oxidation) comparable to that of Pt/Al₂O₃-S (423 K for both CO and C₃H₆ oxidation), and significantly lower than those over the Pt/B-S (444 K for CO conversion and 465 K for C₃H₆ oxidation) and Pt/C-S (487 K for CO and C₃H₆ oxidations) catalysts. The differences (ΔT_{50}) of the 50% CO conversion temperature for the Pt/Al₂O₃, Pt/A, Pt/B, and Pt/C catalysts after and before sulfiding were calculated, and found to increase in the order of Pt/Al₂O₃ (41 K) < Pt/A (51 K) < Pt/B (73 K) < Pt/C (100 K). These results clearly showed that the Pt/A catalyst had excellent sulfur resistance and activity as compared to the Pt/Al₂O₃ catalyst.

We also examined the catalytic activities of all the regenerated catalysts obtained by in situ H₂ reduction at 823 K. These are shown in Fig. 2(c) and (f). After the sulfided Pt/CeO₂-ZrO₂-La₂O₃ catalysts were regenerated in a H₂ atmosphere at 823 K for 1 h, the activities of the catalysts

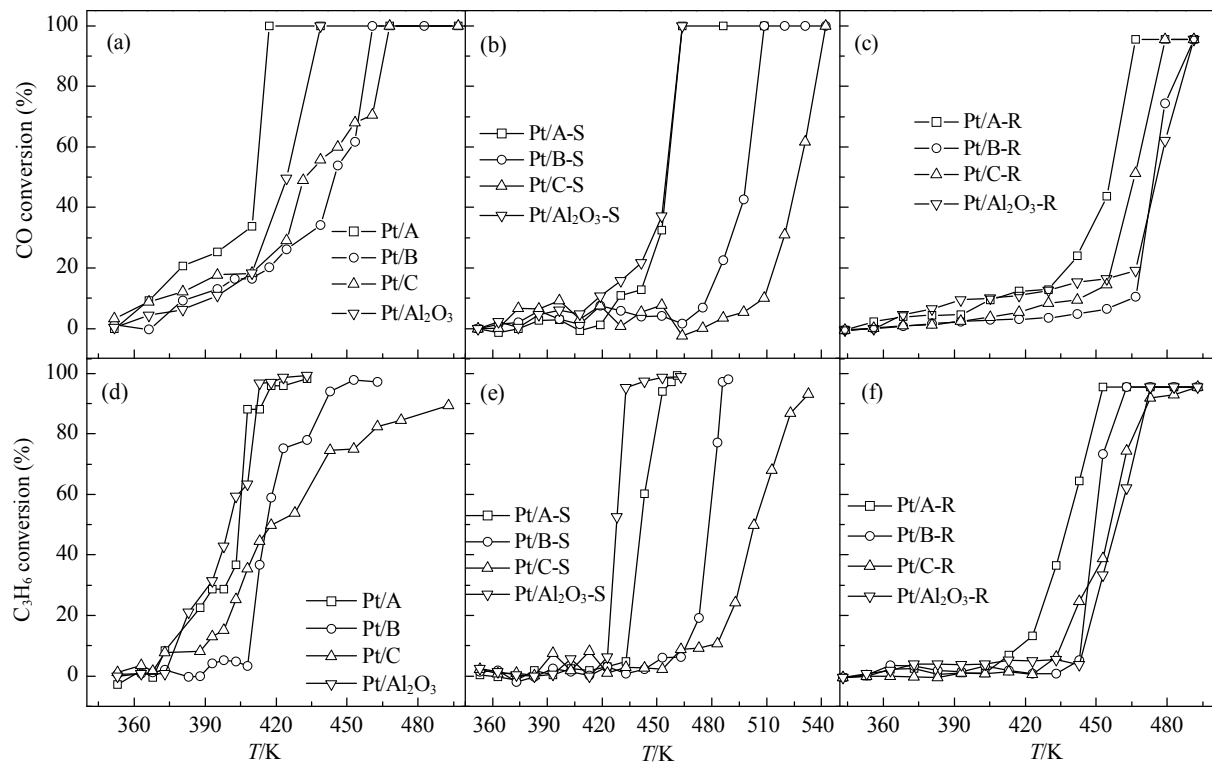


Fig. 2. CO and C₃H₆ conversion over the non-sulfated (a, d), sulfated (b, e), and regenerated (c, f) catalysts.

for both CO and C₃H₆ oxidation were improved. The Pt/A-R catalyst showed a light-off temperature of 423 K for the oxidation of CO and C₃H₆, which was lower than those of the Pt/B-R (443 K) and Pt/C-R (433 K) catalysts. It was interesting to note that the Pt/Al₂O₃-R catalyst exhibited poorer activities for the oxidation of CO and C₃H₆ than the Pt/Al₂O₃-S catalyst. Its light-off temperature was instead increased from 423 to 443 K. This may be due to the agglomeration of active Pt atoms at the high reduction temperature. The H₂ reduction at 823 K did not remove sulfur species bonded to Pt sites. This was confirmed by the TPR-MS results.

2.3 IR spectroscopy

To understand the sulfur-poisoning mechanism, we used IR spectroscopy to characterize the sulfated catalysts. It is well-known that SO₂ oxidation on ceria gives rise to two types of sulfate: surface and bulk-like species. The former is characterized by IR bands in the 1400–1340 cm⁻¹ range while the latter has a very broad band near 1200 cm⁻¹ [23,24]. As seen in Fig. 3, no absorption band in the region of 1700–800 cm⁻¹ was observed for all of the non-sulfated Pt/CeO₂-ZrO₂-La₂O₃ samples. However, after sulfiding, a broad absorption band appeared at 1160 cm⁻¹, indicating that sulfate existed in the form of bulk-like sulfate species. By comparing the intensity of the 1160 cm⁻¹ band, one can

find that the amount of bulk sulfate species formed on the Pt/A sample was the least of the three catalysts. This was consistent with the catalytic results reported above.

2.4 XPS analysis

Figure 4 shows the XPS results on the chemical states of Pt and S. Table 2 lists the characteristics of the non-sulfated and sulfated Pt/CeO₂-ZrO₂-La₂O₃ catalysts deduced from

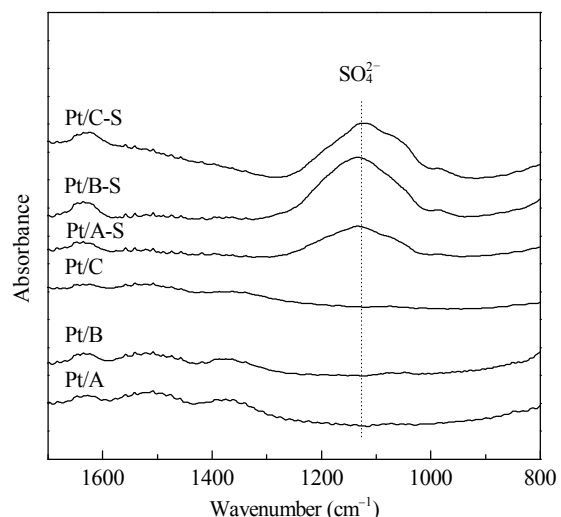


Fig. 3. IR spectra of the Pt/CeO₂-ZrO₂-La₂O₃ catalysts before and after sulfiding.

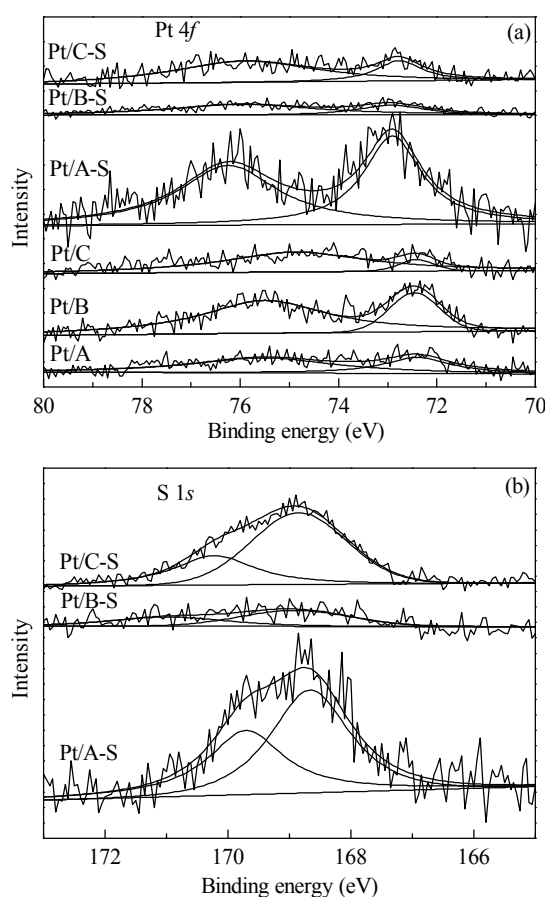


Fig. 4. Pt 4f (a) and S 1s (b) XPS profiles of the non-sulfated and sulfated Pt/CeO₂-ZrO₂-La₂O₃ catalysts.

the XPS investigation. There was no difference in the binding energies (BE) of Ce, Zr, La, and O atoms for the Pt/A, Pt/B, and Pt/C samples. The surface atomic ratio of Ce to Zr for the three samples estimated using photoelectron cross-sections calculated by Scofield showed a moderate difference that depended on the synthesis procedure (seen from Table 2). The surface Ce/Zr ratio of Pt/A was smaller than that of Pt/B, which was comparable with that of Pt/C. The Ce/Zr atomic ratios of all samples were lower than their nominal values, and the surface concentration of Zr was higher than its bulk concentration. This showed that Ce, Zr, and La were not uniformly distributed in the oxides.

The BE of Pt 4f was between 72.3 to 72.5 eV for the non-sulfated samples, indicating that Pt existed in the form of PtO [25]. But after sulfur treatment, the BE of Pt²⁺ was shifted by 0.5 eV towards higher energy, showing a strong electron withdrawing effect derived from the sulfate species revealed by the BE of the S 2p_{3/2} at 168.9 eV [26] and the IR results reported above.

2.5 TPD and TPR analyses

Figure 5(a) shows the CO-TPD profiles of the Pt/A, Pt/B, Pt/C, Pt/A-S, Pt/B-S, and Pt/C-S catalysts. The non-sulfated Pt/A, Pt/B, and Pt/C catalysts showed two broad peaks at 400–800 and 800–1050 K. The intensity of the first desorption peak decreased in the order of Pt/A > Pt/B > Pt/C,

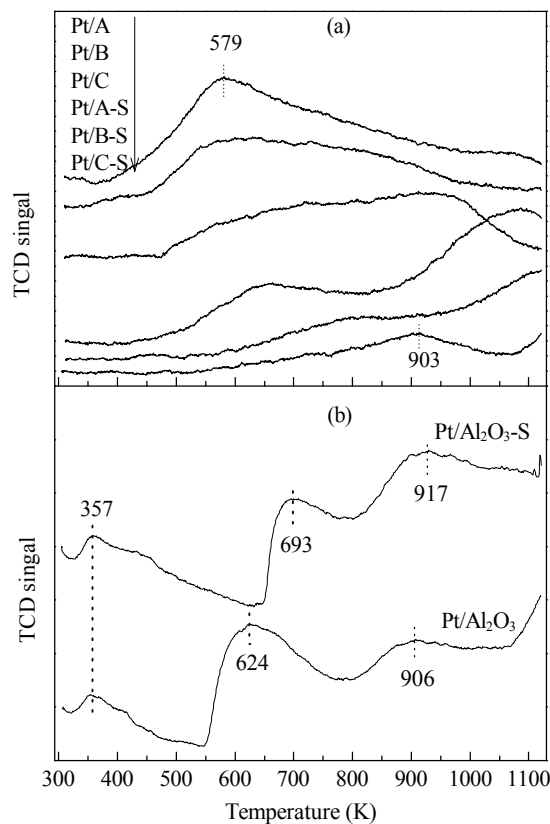


Fig. 5. CO-TPD profiles of the Pt/CeO₂-ZrO₂-La₂O₃ (a) and Pt/Al₂O₃ (b) catalysts before and after sulfation.

Table 2 Characteristic parameters from XPS spectra of non-sulfated and sulfated Pt/CeO₂-ZrO₂-La₂O₃ catalysts

Sample	Binding energy (eV)					Ce/Zr atomic ratio	
	O 1s	Zr 3d _{5/2}	Ce 3d _{5/2}	Pt 4f _{7/2}	S 2p _{3/2}	Theoretical	Experimental
Pt/A	528.8, 530.8	181.5	881.3	72.4	—	1.25	0.33
Pt/A-S	529.5, 531.7, 532.6	182.1	882.1	72.9	168.7	1.25	0.28
Pt/B	528.8, 530.9	181.5	881.6	72.5	—	1.25	0.57
Pt/B-S	529.3, 531.6, 533.8	181.8	882.2	72.9	168.9	1.25	0.66
Pt/C	529.1, 531.1	181.6	881.9	72.3	—	1.25	0.37
Pt/C-S	529.6, 531.6, 533.6	182.1	882.2	72.8	168.9	1.25	0.31

while the second desorption peak increased in intensity in the opposite order. The two broad peaks of the three Pt/CeO₂-ZrO₂-La₂O₃ catalysts were ascribed to CO adsorbed on different Pt sites or partially on CeO_x. This assignment was based on the CO desorption temperatures being comparable to those of the reference catalyst Pt/Al₂O₃ (Fig. 5(b)) where there were two desorption peaks at 624 and 906 K. For Pt/Al₂O₃-S, the CO desorption temperature was clearly increased by sulfur poisoning. This likely resulted from the agglomeration of Pt atoms or that the Al₂(SO₄)₃ formed partially covered Pt particles causing the increase of the CO desorption temperature.

Table 1 shows that the dispersion of Pt on CeO₂-ZrO₂-La₂O₃ decreased in the order of Pt/A > Pt/B > Pt/C. This was the same as with the catalytic activity. After sulfiding, the CO-TPD profiles were two completely separated desorption peaks at low and high temperatures. The intensity of the CO desorption peak at the low temperature for the sulfated catalysts was drastically reduced, indicating that the amount of CO adsorbed on Pt sites decreased due to the poisoning of the Pt surface by sulfur. Moreover, the desorption temperature of CO adsorbed on Pt increased in the order of Pt/A-S < Pt/B-S < Pt/C-S, while the intensity of the CO desorption peak decreased in the order of Pt/A-S > Pt/B-S > Pt/C-S.

The TPR results shown in Fig. 6 gave information on the desulfurization characteristics of Pt/A-S, Pt/B-S, Pt/C-S, and Pt/Al₂O₃-S. No H₂S desorption was observed from Pt/Al₂O₃-S in the temperature range of 563 to 900 K. This, together with the XRF analysis result, indicated that the sulfur bonded to the Pt sites was irreducible. Compared with the peak intensity of the H₂S fragment of the Pt/CeO₂-ZrO₂-La₂O₃ catalysts, one can find that the Pt/A-S sample contained the least amount of reducible SO₄²⁻. This may be attributed to the different surface Ce/Zr ratios. Because of

the strong surface basicity and the unique feature of the storage and release oxygen of CeO₂, it was more active in the adsorption and oxidation of the acidic SO₂ as compared to ZrO₂. Thus, a large Ce/Zr ratio indicated more storage capacity of sulfur. The results of the catalytic activity evaluation showed that the regeneration treatment for the Pt/CeO₂-ZrO₂-La₂O₃ samples improved the catalytic activity for both CO and C₃H₆ oxidation. This suggested that the reducible sulfur species bonding with the support was not the key factor deactivating the catalyst. Considering that the reduction regeneration significantly increased the light-off temperature of CO and C₃H₆ oxidation over the Pt/Al₂O₃-S sample, which did not have reducible sulfur species, one can conclude that the poisoning of the Pt surface was mainly responsible for the deactivation of the sulfated Pt/CeO₂-ZrO₂-La₂O₃ catalysts. Moreover, since the sulfur poisoning caused a textural change of the Pt/CeO₂-ZrO₂-La₂O₃ catalysts, a small part of the Pt particles was possibly buried into the bulk of the CeO₂-ZrO₂-La₂O₃ support. This may be one factor causing the deactivation.

3 Conclusions

The synthesis procedure affected Pt/CeO₂-ZrO₂-La₂O₃ catalysts with the same composition and gave significant differences in structure, texture, sulfurization-desulfurization behavior, and catalytic behavior. The Pt/CeO₂-ZrO₂-La₂O₃ catalyst with the larger surface Ce/Zr ratio had more sulfur poisoning, and consequently a higher light-off temperature for the catalytic removal of pollutants in simulated diesel exhaust gas. The deactivation was mainly due to the poisoning of Pt surface by sulfur. The CeO₂-ZrO₂-La₂O₃ oxide with a Zr-rich surface gave a good dispersion of Pt, and hence excellent catalytic activity and sulfur tolerance.

References

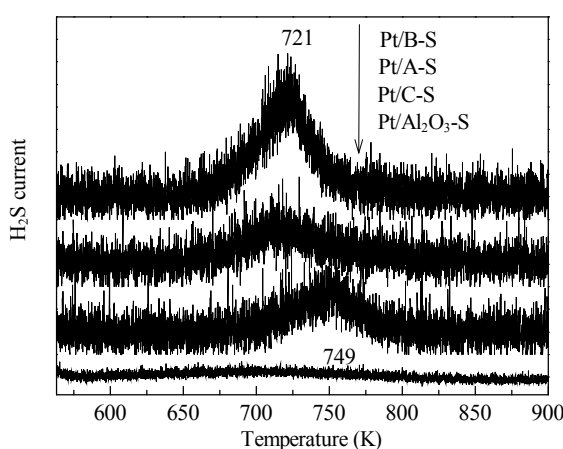


Fig. 6. TPR profiles of the sulfated Pt/CeO₂-ZrO₂-La₂O₃ and Pt/Al₂O₃ catalysts.

- 1 张桂臻, 韩丽艳, 赵震, 刘坚, 段爱军, 姜桂元. 现代化工 (Zhang G Zh, Han L Y, Zhao Zh, Liu J, Duan A J, Jiang G Y. *Mod Chem Ind*), 2008, **28**(1): 35
- 2 Agarwal A K. *Prog Energy Combust Sci*, 2007, **33**: 233
- 3 Hosoya M, Shimoda M. *Appl Catal B*, 1996, **10**: 83
- 4 Farrauto R J, Voss K E. *Appl Catal B*, 1996, **10**: 29
- 5 Stein H J. *Appl Catal B*, 1996, **10**: 69
- 6 Liu J A, Xu J, Zhao Zh, Duan A J, Jiang G Y, Jing Y N. *J Environ Sci (China)*, 2010, **22**: 1104
- 7 Haneda M, Houshito O, Takagi H, Shinoda K, Nakahara Y, Hiroe K, Fujitani T, Hamada H. *Top Catal*, 2009, **52**: 1868
- 8 Kim J R, Myeong W J, Ihm S K. *J Catal*, 2009, **263**: 123
- 9 Haneda M, Shinoda K, Nagane A, Houshito O, Takagi H, Nakahara Y, Hiroe K, Fujitani T, Hamada H. *J Catal*, 2008, **259**: 223

- 10 Atribak I, Bueno-López A, García-García A. *J Catal*, 2008, **259**: 123
- 11 Kollil T, Huuhtanen M, Hallikainen A, Kallinen K, Keiski R L. *Catal Lett*, 2009, **127**: 49
- 12 Kollil T, Kanerva T, Lappalainen P, Huuhtanen M, Vippola M, Kinnunen T, Kallinen K, Lepistö T, Lahtinen J, Keiski R L. *Top Catal*, 2009, **52**: 2025
- 13 Kollil T, Kanerva T, Huuhtanen M, Vippola M, Kallinen K, Kinnunen T, Lepistö T, Lahtinen J, Keiski R L. *Catal Today*, 2010, **154**: 303
- 14 Trovarelli A. *Catal Rev-Sci Eng*, 1996, **38**: 439
- 15 Aneggi E, de Leitenburg C, Dolcetti G, Trovarelli A. *Catal Today*, 2006, **114**: 40
- 16 Setiabudi A, Chen J, Mul G, Makkee M, Moulijn J A. *Appl Catal B*, 2004, **51**: 9
- 17 Bazin P, Saur O, Meunier F C, Daturi M, Lavalle J C, Le Govic A M, Harlé V, Blanchard G. *Appl Catal B*, 2009, **90**: 368
- 18 Rohart E, Bellière-Baca V, Yokota K, Harlé V, Pitois C. *Top Catal*, 2007, **42-43**: 71
- 19 Si R, Zhang Y W, Wang L M, Li S J, Lin B X, Chu W S, Wu Z Y, Yan C H. *J Phys Chem C*, 2007, **111**: 787
- 20 Zhong F L, Xiao Y H, Weng X M, Wei K M, Cai G H, Zheng Y, Zheng Q. *Catal Lett*, 2009, **133**: 125
- 21 Joly V L J, Joy P A, Date S K. *J Magn Magn Mater*, 2002, **247**: 316
- 22 郭大为. 石油学报(石油加工)(Guo D W. *Acta Petrol Sin (Petrol Process Sect)*), 2010, **26**: 235
- 23 Luo T, Gorte R J. *Appl Catal B*, 2004, **53**: 77
- 24 Waqif M, Bazin P, Saur O, Lavalle J C, Blanchard G, Touret O. *Appl Catal B*, 1997, **11**: 193
- 25 Huang M H, Li L R, Guo Y L. *J Soild State Electrochem*, 2009, **13**: 1403
- 26 Corro G, Fierro J L G, Odilon V C. *Catal Commun*, 2003, **4**: 371